JOURNAL OF OPTOELECTRONICS AND ADVANCED MATERIALS Vol. 12, No. 5, May 2010, p. 1078 - 1082

Stress and texture in titanium nitride thin films by X-ray diffraction techniques

C. DUCU*, S. MOGA, D. NEGREA, V. MALINOVSCHI, M. BALACEANU[a]
University of Pitesti – Research Center for Advanced Materials, Pitesti, Romania
[a]National Institute for Optoelectronics – INOE 2000, Bucharest, Romania

In this paper we used X-Ray diffraction techniques in order to study the microstructural parameters of TiN thin films deposited on silicon substrate by cathodic arc method. In terms of preferred orientation, the texture for all TiN thin films can be described as <111> || normal direction fiber texture. The residual stresses were evaluated using the crystallite group method, applicable for specimens exhibiting a crystallographic fiber texture being simultaneously strong and sharp.

(Received August 20, 2009; accepted May 26, 2010)

Keywords: X-ray diffraction, Thin films, Texture, Residual stress

1. Introduction

The high hardness and chemical inertness, excellent wear-corrosion resistance are the key qualities for the wide use of B1-structure titanium nitride (TiN) coatings. As it is well known, the performance and lifetime of hard coatings depend on important parameters such microstructure, crystallographic texture and residual stress [1-3].

X-ray diffraction (XRD) is a strong tool for the structural analysis of hard coatings. Crystalline structure, grain size, microstrain, texture, phase composition and residual stress are the most important film characteristics that are commonly determined by XRD technique (e.g. [4-6]).

In the work presented here, XRD analysis was used to determine lattice parameters, phase composition, texture and residual stress of TiN thin films prepared by the cathodic arc method under different ion bombardment conditions.

1.1 Crystallographic texture of thin films

Texture development in polycrystalline thin films has been extensively studied. Generally, the models to explain the mechanisms controlling the texture take into account thermodynamic and/or kinetic driving forces [7-12]. In the case of thermodynamic effects, the preferred orientation is considered to be dictated by the condition of minimization of the overall film energy, that is the sum of surface and strain energy [8,9]. Kinetic driving forces are related to anisotropies in adatom mobility's, surface diffusivities and collisional cascade effects [12]. Two kinds of textures play prominent roles in thin film technology: the fiber-texture and the biaxial-texture [6]. A series of methods are usually used to investigate texture of polycrystalline thin films: calculation of texture factors, ω-scan (rocking curves) measurements, ϕ-scan and pole figures measurements of certain X-ray diffraction lines. In the case of polycrystalline thin films, the anisotropy of crystallite orientation is often encountered. This phenomenon can be recognized, in an early stage, from the departure of intensity ratios in a symmetrical X-ray diffraction pattern corresponding to the thin film sample from the intensity ratios of a powder pattern with random orientation. X-ray texture analysis is typically performed by means of Schulz reflection method [13].

1.2 Residual stress measurement

X-ray diffraction is commonly used to measure the stress state in thin films. From the angular positions of diffraction lines one can derive the lattice spacing's and used them to calculate the elastic lattice strains (diffraction strain) [14,15]. By means of Hooke's law and material elastic constants, the elastic strains can be related to the stress tensor. Even in absence of texture, thin films cannot generally be considered as macroscopically elastically isotropic [16,17], therefore the classical $\sin^2\psi$ method [18] is not a suitable method for X-Ray diffraction stress analysis of thin film samples. Special procedures, such as the Crystallite Group Method (CGM) [19-21] or the use of X-Ray stress factors [22], have been proposed for the diffraction stress analysis of specimens exhibiting distinct macroscopic anisotropy due to texture. Residual stress measurements based on the CGM was preferred since the analyzed TiN thin films exhibit strong fiber-textures.

The CGM was proposed for diffraction stress analysis of materials with strong texture components and was also adapted to fiber-textured specimens [19,23,24]. In order to perform the stress analysis several different *hkl* reflections are measured. The presence of crystallographic texture implies the measurement of *hkl* reflections only at certain tilt angles with respect to the preferred orientation of the analyzed crystallite group, dependant on the material structure. The CGM can be employed even for rather weak texture [25], this method leading to a linear dependence of measured diffraction strain on $\sin^2\psi$

[26]. Also, in the case of {111} and {001} fiber-textures of cubic materials, the method does not take into account the elastic grain interaction, the measured strains being related to the stresses by the single-crystal elastic constants of the material [27]. For a rotationally symmetric biaxial state of stress the non-zero components of the stress tensor are $\sigma_{11} = \sigma_{22} = \sigma_{\parallel}$ $(\sigma_{\perp} = 0)$. The simplified $\sin^2\psi$ - law for cubic symmetry in the presence of {111} fiber texture, reduces to [28]:

$$\varepsilon_{\psi}^{111} = \frac{a_{\psi}^{111} - a_0^{111}}{a_{\psi}^{111}} = \left(2s_{12} + \frac{2}{3}s_0 + \frac{1}{2}s_{44}\sin^2\psi\right)\cdot\sigma_{\parallel}, \qquad (1)$$

where s_{ij} represents the elastic compliance tensor of the material in the Voigt notation and $s_0 = s_{11} - s_{12} - s_{44}/2$ is the anisotropy factor of the material.

The relation (1) leads to the expression of the lattice parameter as a function of orientation:

$$a_{\psi}^{111} = a_0 \cdot \left[1 + \left(2s_{12} + \frac{2}{3}s_0 + \frac{1}{2}s_{44}\sin^2\psi\right)\cdot\sigma_{\parallel}\right] \qquad (2)$$

From the condition $a_{\psi} = a_0$, the so-called "strain-free direction" (noted $\sin^2\psi^*$) can be obtained. For {111} fiber texture its expression is:

$$\sin^2\psi^* = 2\left(-2s_{12} - 2/3s_0\right)/s_{44}. \qquad (3)$$

The strain-free direction depends only on the elastic constants of the material and a value of ~0.41 was obtained using the elastic stiffness constants calculated by Nagao [29].

2. Experimental

2.1 Sample preparation

The TiN films were deposited on Si wafers by the cathodic arc method. The experimental set-up for the film deposition was described elsewhere [30]. The deposition chamber was equipped with two Ti cathodes (99.99% purity) and the reactive atmosphere was a mixture of N_2 and Ar gases. The base pressure before deposition was 6×10^{-4} Pa, while the working gas (N_2+Ar) pressure was of about 8×10^{-2} Pa. Prior to deposition, the wafers were ultrasonically pre-cleaned and treated with Ar plasma for 10 min at RF substrate bias. To examine the influence of the energy of the film characteristics as resulted from the XRD analysis, the applied substrate bias V_s was varied from -200 to -500 V. The other process parameters were as follows: N_2 flow rate -80 sccm; Ar flow rate – 15 sccm; arc current (at both cathodes) – 110 A; substrate temperature during deposition – from 320 to 390°C (depending on V_s); deposition time ~ 40 min. The overall thickness of all films was controlled to be of about 1.8 μm.

2.2 X-ray diffraction measurements

All the X-ray diffraction measurements were performed on a Rigaku Ultima IV system (CuK_α radiation) with parallel beam optics. The divergence angle of emitted beam from the multilayer mirror is approximately 0.05^0. This kind of optics is suitable for thin film analysis, especially for texture and residual stress measurements, because of increased beam intensity and significant reduction of instrumental aberrations (the preservation of peak position, shape and width even at high ψ - tilting angles) [28].

For the qualitative phase analysis the X-ray diffraction patterns were recorded in Bragg-Brentano geometry, in the 2θ range 30^0-150^0, step width 0.05^0 and 10s as counting time. The texture analysis was performed using a multipurpose attachment for pole figure measurements. The measurements for residual stress determination were recorded in high precision-high resolution mode (parallel beam optics, parallel slit analyzer collimator in the receiving side with 0.114^0 acceptance angle), with a step width of 0.05^0 and a counting time of 20s per step.

3. Results and discussion

3.1. Phase composition and texture

The recorded symmetrical θ/2θ X-ray diffraction patterns for TiN thin films are shown in figure 1. The intensity is plotted in logarithmic scale. TiN coatings were polycrystalline exhibiting reflections related to B1 cubic structure. The (101) reflection of Ti_α was detected in all the X-ray diffraction patterns. From the patterns we can observe that the X-ray diffraction lines had apparently shifted from the positions corresponding to a randomly oriented strain-free standard TiN sample (dashed lines in the figure). This indicated that the coatings are subjected to a residual stress state. Also the intensities of TiN reflections are very different from those of a randomly oriented sample. Therefore we can conclude that the samples have crystallographic planes with preferred orientation.

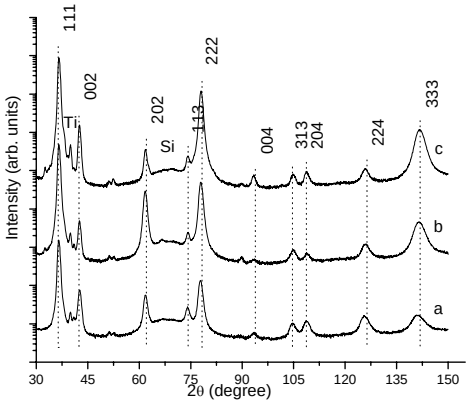

Fig. 1. X-ray diffraction patterns for TiN thin films deposited at different applied substrate bias: a: –200 V, b: -300V, c: -500V.

The ϕ-scan measurements (not shown here) revealed the presence of fiber-texture (the intensity is independent of azimuth angle, ϕ). Therefore we can study the preferred orientation by Ψ-tilt measurements of diffracted intensity at constant ϕ sample rotation. In the case of thin films, the peak maximum measured for a certain value of Ψ may shift for another value due to residual stress state in thin films. For this reason the integral intensity measurement for each orientation ($\theta/2\theta-\Psi$ scans) [31] was preferred to Schultz reflection method.

TiN (111) reflection was measured in its specific 2θ range, 0.05^0 step width and 10s time per step for each value of tilt range 0^0-82^0. The measured integral intensities of the (111) reflection at different Ψ-tilt (2^0 increment) were corrected for absorption factor [6]. Fig. 2 shows normalized intensity versus tilt angle Ψ ($\phi=0$) for (111) reflection of analyzed samples.

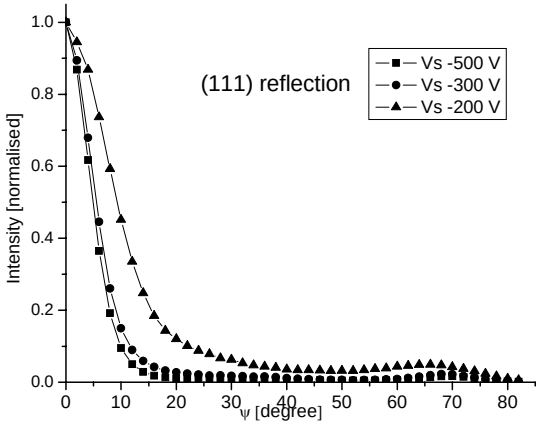

Fig. 2. Integrated intensity of the (111) reflection as a function of tilt angle for the three thin films (values corrected for absorption factor).

In general, two maxima can be observed: one at $\psi\approx 0^0$ and one at $\psi\approx 70.5^0$. The peak at $\psi\approx 0^0$ indicates the presence of a strong <111>||ND (normal direction) fiber texture. The (111) texture was reported for various types of films (TiN, CrN, NbN, NbC, TiAlN, TiCN, TiAlZrCN) deposited by cathodic arc technique [32-36]. The presence of a highly ionized plasma, specific to this method, was considered to favor the film growth in the most densely packed direction (i.e. (111) direction) [35].

The position of the second maximum at high ψ-tilt values corresponds to the angle between (111) and $(\bar{1}11)$ planes in the cubic structure.

Pole widths (half widths at 0.5 normalized intensity for $\psi=0^0$) were calculated by fitting the curves with bell-shaped pseudo-Voigt functions. Plot of pole widths vs. applied substrate bias (figure 3) shows high texture sharpness for -500 V and -300 V applied substrate bias. For the -200 V applied substrate bias, the second maximum (as can be seen in figure 2) is shifted towards lower values. Considering this feature and the broader texture we can assume that a mixed [111]/[211] texture is present, since (111) planes of fcc structures form deformation twins along [211] [37,38].

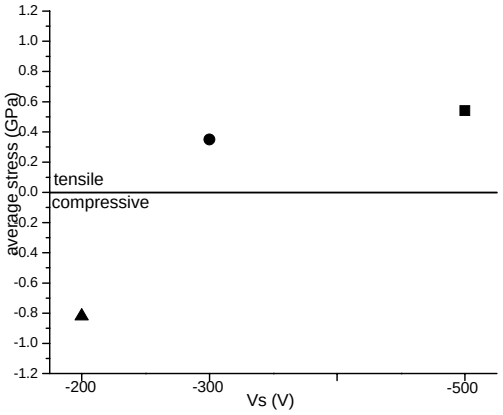

Fig. 3. Pole widths of (111) reflection plotted as a function of applied substrate bias.

Assuming that regions in the plot are associated with a single fiber-texture component, then integration can be performed to find the area under the curve. We can obtain the volume fraction as the sum of the associated areas divided by the total area. By integrating the curves we have found that the random component (crystallites not belonging to {111} fiber) is 4% in the case of Vs = - 500 V and 7% for the Vs = - 300 V.

3.2. Residual stress

The crystallographic texture measurements revealed the presence of strong {111} fiber textures for all the samples. The texture is also sharp (excepting the sample deposited at -200 V applied substrate bias), all these findings enabling the use of CGM for stress determination. Because of strong texture, we can measure the intensity only for few Ψ values with respect to {111} crystallite group. These values are presented in table 1.

Table 1. Tilt angles corresponding to {hkl} poles with respect to [111] direction.

[111]										
{hkl}	222	224	313	113	202	204	002	113	111	113
Ψ (^{0})	0	19.5	22	29.5	35.3	39.2	54.7	58.5	70.5	80

The residual stress analysis was performed on {111} crystallite group of TiN thin films.

The $\sin^2\psi$ plots of TiN thin films are shown in figure 4. The lattice parameter values were obtained from the peak maximum positions using the Bragg's law and the relationship between lattice parameters, Miller indices and lattice spacing for cubic materials.

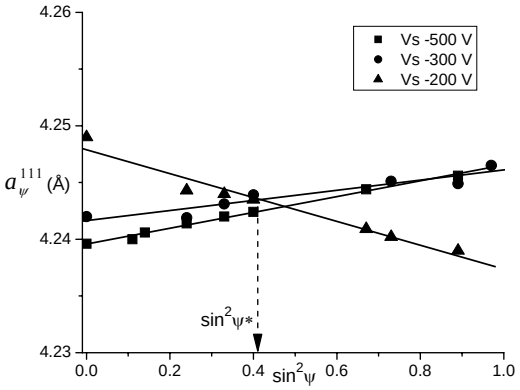

Fig. 4. GCM $\sin^2\psi$ *plots on [111] oriented grains.*

We can observe in the figure that the variation of a_ψ vs. $\sin^2\psi$ has a linear behavior.

The "strain-free lattice parameters" were calculated using the a_ψ^{111} values by interpolating at the strain-free direction calculated above (3), assuming a rotationally symmetric biaxial state of stress. The values obtained (~4.24 Å) are in reasonable agreement with the TiN bulk value (4.242 Å).

A change in the sign of the residual stress with the increase of the applied substrate bias can be observed. For polycrystalline films, transition from compressive to tensile stresses could be related to the grain boundary relaxation processes (see, e.g. [39]). An increase in the ion bombardment energy causes modifications in intercolumnar spaces and gaps between grains, leading to the enhancement of the intragrain tensile forces. In order to obtain quantitative information on stress, data were fitted using the symmetric biaxial stress model, and fit lines are reported in Fig. 4.

Fig. 5 shows the calculated average residual stress values as a function of applied substrate bias.

It has to be noticed that our measurements do not take into account the presence of a stress gradient in the analyzed samples. Thus the obtained values are average values within the layers, used for comparison purposes [37].

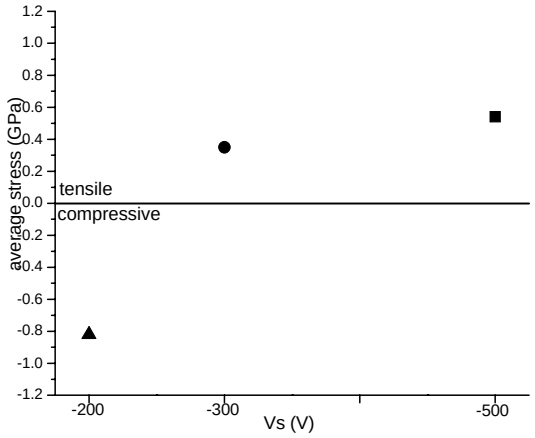

Fig. 5. Residual stress of TiN coatings vs bias voltage.

4. Conclusions

Titanium nitride thin films deposited by the cathodic arc method have been characterized by X-ray diffraction for the determination of crystallographic texture and macrostresses within the films. The structural analysis shows that TiN coatings are polycrystalline exhibiting reflections related to B1 cubic structure.

The $\theta/2\theta-\Psi$ scans revealed the presence of a strong and sharp <111>||ND (normal direction) fiber texture. Diffraction stress analysis performed on {111} crystallite group of TiN thin films by means of CGM indicates a change in the sign of residual stress as a function of applied substrate bias. Strain-free lattice parameters obtained for all thin films are in good agreement with TiN bulk value. Therefore we can assume that the symmetric biaxial stress model is a valid model for our samples.

Acknowledgements

This work is a part of the Romanian National R&D Plan II 2007-2013 financed by the Ministry of Education, Research and Innovation, under research project No. 71-038/2007.

References

[1] Handbook of refractory carbides and nitrides: properties, characteristics, processing, and applications, William Andrew, ed. Hugh O.Pierson, Noyes Publications (1996).
[2] D. S. Stone, K. B. Yoder, W. D. Sproul, J. Vac. Sci. Technol. A **9**, 2543 (1991).
[3] P. Patsalas, C. Charitidis, S. Logothetidis, Surf.&Coat.Technol. **125**, 335-339 (2000).

[4] J. E. Sundgren, A. Rockett, J. E. Greene, U. Helmersson, J. Vac. Sci. Technol. A **4**(6), 2770 (1986).
[5] Springer Handbook of Materials Measurements Methods, H.Czichos, T.Saito, L.Smith (Eds), Springer Science, Leipzig (2006).
[6] Thin Film Analysis by X-Ray Scattering, M.Birkholz, Wiley-VCH, 183-237 (2006).
[7] B. Rauschenbach, J. W. Gerlach, Cryst. Res. Technol. **35**, 675 (2000).
[8] J. Pelleg, L. Z. Zevin, S. Lungo, N. Croitoru, Thin Solid Films **197**, 117 (1991).
[9] U. C. Oh, Jung Ho Je, J. Appl. Phys. **74** (3), 1692 (1993).
[10] D. Gall, S. Kodambaka, M. A. Wall, I. Petrov, J. E. Greene, J. Appl. Phys. **91**, 3589 (2002).
[11] S. Mahieu, P. Ghekiere, G. De Winter, S. Heirwegh, D. Depla, R. De Gryse, O. I. Lebedev, G. Van Tendeloo, J. Cryst. Growth **279**, 100 (2005).
[12] G. Abadias, Y. Y. Tse, Ph. Guérin, V. Pelosin, J. Appl. Phys. 99, 113519-1 (2006).
[13] L. G. Schulz, J. of Appl. Phys. **20,** 1030 (1949)
[14] I. C. Noyan and J. B. Cohen, Residual Stress. Measurement by Diffraction and Interpretation Springer, New York, (1987)
[15] V. Hauk ed., Structural and Residual Stress Analysis by Nondestructive Methods, Elsevier, Amsterdam, (1997).
[16] M. van Leeuwen, J.-D. Kamminga, E. J. Mittemeijer, J. Appl. Phys. **86**, 1904 (1999)
[17] U. Welzel, M. Leoni, E.J. Mittemeijer, Philosophical Magazine **83:5**, 603 (2003)
[18] E. Macherauch, P. Müller, Z. Angew. Phys. **13**, 305 (1961).
[19] V. Hauk, R. Oudelhoven,. Z. Metallkd. **79**, 41 (1988).
[20] P. F.,Willemse, B. P. Naughton, C. A. Verbraak. Mater. Sci. Eng. **56**, 25 (1982).
[21] P. F. Willemse B. P. Naughton. Mater. Sci. Technol. **1**, 41 (1985).
[22] U. Welzel, E.J. Mittemeijer, J. Appl. Phys. **93**, 9001 (2003).
[23] V. Hauk, G. Vaessen, Z. Metallkd. **76**, 102 (1985).
[24] H. U. Barron, V. Hauk, Z. Metallkd. **79**, 127 (1988).
[25] P. Gergaud, S. Labat, O. Thomas, Thin Solid Films **319,** 9–15 (1998)
[26] J. Pina, A. Dias, M. Francois, J.L. Lebrun, Surface and Coatings Technology **96,** 148 (1997)
[27] U. Welzel, J. Ligot, P. Lamparter, A. C. Vermeulen E. J. Mittemeijer, J. Appl. Cryst. **38**, 1 (2005).
[28] A. Kumar, U. Welzel, E.J. Mittemeijer, Z. Kristallogr. Suppl. **23,** 55-60 (2006)
[29] S. Nagao, K. Nordlund, R. Nowak, Phys. Rev. B **73,** 144113 (2006)
[30] A. Vladescu, A. Kiss, A. Popescu, M. Braic, M. Balaceanu, V. Braic, I. Tudor, C. Logofatu, C. C. Negrila, R. Ripeanu, J.Nanosci. Nanotechnol., **8,** 717 (2008)
[31] P. Scardi, M. Leoni, M. D'Incau, Thin Solid Films **467,** 326 (2004)
[32] V. N. Zhitomirsky, I. Grimberg, L. Rapoport, R. L. Boxman, N. A. Travitzky, S. Goldsmith, B. Z. Weiss, Surf. Coat. Technol., **133-134,** 114 (2000)
[33] W. K. Grant, C. Loomis, J. J. Moore, D. L. Olson, B. Mcshra. A.J. Perry, Surf. Coat. Technol. **86-87**, 788 (1996)
[34] A. Bendavid, P. J. Martin, T. J. Kinder, E. W. Preston, Surf. Coat. Technol. **163-164**, 347 (2003)
[35] D. C. Kothari, A. N. Kale, Surf. Coat. Technol. **158-159**, 174 (2002).
[36] M. Balaceanu et al., Surf. Coat. Technol. **202,** 3981 (2008)
[37] M. Leoni, P. Scardi, S. Rossi, L. Fedrizzi, Y. Massiani, Thin Solid Films **345,** 263 (1999)
[38] D. B. Cullity, Elements of X-ray Diffraction, Addison-Wesley, Reading, MA (1974).
[39] Y. Pauleau, in: Tribology of diamond-like carbon films, C.Donnet, A.Erdemir (Eds), Springer Science, New York (2008)

*Corresponding author: catalin.ducu@upit.ro